

An Accurate Beam-Tracking Algorithm with Adaptive Beam Reconstruction via UAV-BSs for Mobile Users

Jing Zhang, *Member, IEEE*, Sheng Gao, Xin Feng, Hongwei Yang, and Geng Sun, *Member, IEEE*

Abstract—Unmanned aerial vehicles (UAVs) with flexible deployment contribute to enlarging the distance of information transmission to mobile users (MUs) in constrained environment. However, due to the high mobility of both UAVs and MUs, it is challenging to establish an accurate beam towards the target MU with high beam gain in real-time. In this study, UAV base stations (UAV-BSs) consisting of position-known assisted UAVs (A-UAVs) and position-unknown assisted UAVs (U-UAVs) are employed to transmit data to MUs. Specifically, a bi-directional angle-aware beam tracking with adaptive beam reconstruction (BAB-AR) algorithm is proposed to construct an optimal beam that can quickly adapt the movement of the target MU. First, the angle-aware beam tracking is realized within the UAV-BSs using a proposed global dynamic crow search algorithm without historical trajectory. Furthermore, the Gaussian process regression model is trained by A-UAVs to predict the azimuth and elevation angles of MUs. Meanwhile, we focus on the beam width and design a time interval adjustment mechanism for adaptive beam reconstruction to track high-speed MUs. Finally, the performance of the BAB-AR algorithm is compared with that of benchmark algorithms, and simulate results verifies that the BAB-AR algorithm can construct an accurate beam capable of covering high-speed MUs with the half power beam width in a timely manner.

Index Terms—beam tracking, angle aware, predictive beam-forming, mobile user.

I. INTRODUCTION

BEAM-TRACKING is a promising technique for real-time transmission of data to mobile users (MUs), offering a high signal-to-noise ratio (SNR) with millimeter wave (mmWave) [1], [2]. For instance, the beam gain for a MU can be increased significantly by quickly reconstructing the beam [3], [4]. In vehicular communication systems, beam tracking enables the transmission of data between the base station (BS) and target MU at high data rate and with dependable service

[5]. However, in remote scenarios such as mountainous areas, the beam-tracking service provided by a BS may be interrupted by tall buildings or plants [6], [7].

In recent years, UAV-BSs have found widespread application in various domains, including civilian and military contexts, to ensure reliable communications for MUs without any environmental constraints [8], [9]. Due to the mobility of UAVs, UAV-BSs can be flexibly deployed to establish a line-of-sight (LoS) communication link [10], [11], thereby providing the long-range information transmission services with high capacity to MUs [12]. However, the mobility of UAVs presents challenges in achieving accurate beam tracking and alignment to MUs. While GPS can provide the locations of MUs and UAVs, its deployment is expensive, and location errors can occur in mobility scenarios. In addition, environmental factors such as wind can affect the locations of UAVs even when they follow pre-set trajectories. To address these challenges, angle-aware beam-tracking algorithms have been proposed to achieve beam tracking for UAV-to-MU links with high accuracy.

The existing angle-aware predictive beam-tracking algorithms that consider angles require the historical trajectory of UAVs, but their accuracy in predicting locations may not be satisfactory for different motion patterns. Furthermore, the reconstruction time of a beam is often overlooked, while beam coverage is a crucial factor in constructing available beams [13], [14]. Previous works have used beam coverage to create wide beams for error domains caused by angular predictions or regions that the pre-set codebook cannot cover. Transmission interruption occurs when the target MU moves outside the beam coverage region. Moreover, the fixed time interval for reconstructing a beam cannot keep up with the speed of MUs. Therefore, it is crucial to reconstruct a beam based on the beam coverage in an adaptive mode.

In order to ensure that the target MU remains within the coverage of the constructed beam, this study employs a combination of position-known assisted UAVs (A-UAV) and position-unknown assisted UAVs (U-UAV). This approach facilitates efficient information transmission to MUs with beam tracking. A novel bi-directional angle-aware beam-tracking with adaptive beam reconstruction (BAB-AR) algorithm is proposed to accurately reconstruct the beam based on the movement of the MU, thereby preventing beam misalignment due to high speed of both MUs and UAVs. Thus, the BAB-AR algorithm can mitigate communication interruptions that may occur due to reconstructing a beam with a fixed time interval.

This research was supported in part by the Jilin Province Science and Technology Development Plan Project (YDZJ202201ZYTS416), and in part by the National Natural Science Foundation of China (62272194). (*Corresponding author: Geng Sun*)

Jing Zhang is with the College of Computer Science and Technology, Changchun University of Science and Technology, Changchun 130022, China, and also with the College of Communication Engineering, Jilin University, Changchun 130012, China (e-mail: zhang_jing@cust.edu.cn).

Sheng Gao, Xin Feng and Hongwei Yang are with the College of Computer Science and Technology, Changchun University of Science and Technology, Changchun 130022, China (e-mail: shenggao.cs@gmail.com; fengxin@cust.edu.cn; yanghongwei@cust.edu.cn).

Geng Sun is with the College of Computer Science and Technology, Jilin University, Changchun 130012, China, and also with the College of Computing and Data Science, Nanyang Technological University, Singapore 639798 (e-mail: sungeng@jlu.edu.cn).

The main contributions of this paper are outlined below.

- A modified global dynamic crow search algorithm (GD-CSA) is proposed for locating U-UAVs without GPS and for realizing accurate angle-aware beam tracking within the UAV-BSs. The GD-CSA incorporates a predetermined optimal point set and a dynamical location updating mechanism to achieve fast convergence to the optimal solution. A-UAVs can cooperatively locate the U-UAVs using GD-CSA, avoiding the need of high-dimensional computation regardless of any UAV's moving patterns.
- A Gaussian process regression (GPR) model is employed to predict the azimuth and elevation angles of the target MU based on the U-UAV's locations, which eliminates frequent pilot overhead. Furthermore, a time interval adjustment mechanism (TIAM) is proposed to calculate an adaptive time interval for reconstructing the beam according to the movement of MUs and the beam width.
- The performance of the proposed BAB-AR algorithm is verified under different movement patterns. Simulation results show that the angle relative error of the GD-CSA is within 0.2 under different motion patterns. Furthermore, BAB-AR achieves higher SNR and transmit rate at MUs compared to that of the angle-aware beam tracking with machine model. When MU moves slowly, energy-efficiency at MU can be improved approximately 136.46% and 215.99% compared to that of the fixed time interval mode and the codebook-based algorithm, respectively.

The rest of this paper is organized as follows. Section II provides an overview of existing literatures on beam tracking for MUs. Section III presents the problem model and channel model used in the proposed scenarios. Section IV describes the process of the proposed algorithm in detail. Section V discusses the results of the simulation experiment, and Section VI concludes this study.

II. RELATED WORK

In this study, UAV-BSs are employed to enable accurate beam tracking for MUs. It is crucial to promptly reconstruct beams for MUs in order to prevent communication interruptions resulting from the high speed of both UAVs and MUs. The following prior works have explored various algorithms to update beam vectors and quickly reconstruct beams to accommodate the mobility of UAVs and MUs. The characteristics of the existing algorithms and this study are summarized in Table I.

Some studies have focused on the codebook-based beam-tracking algorithms and developed various hierarchical multi-resolution codebooks to mitigate the impact on beam alignment caused by the high mobility of both MUs and UAVs [13], [15], [16]. These algorithms initially designed and established the codebook, after which UAVs and MUs can select the optimal beam vector from the fixed codebook. The codebook-based beam-tracking algorithm minimizes the time required for beam training and beam vector selection. However, the fixed codebook lacks the ability to independently and promptly adapt to align with the target MU, resulting in suboptimal

beam gain. Moreover, despite the continuity of the codebook, uncovered regions always exist due to the difference between the spatial frequency and geographic domains, which leads to communication interruptions between the UAVs and MUs [17].

Another solution is the beam vector-optimized beam-tracking algorithms. An alternating interference suppression algorithm [18] was proposed to maintain UAVs' communication. By optimizing the beam vector for both the link between the BS and UAVs and the link between UAVs and MUs. This approach maximized the beam gain of the target signal while effectively mitigating interference. In [19], the least square algorithm was employed to optimize the beam vectors for UAVs and MUs, resulting in a cooperative sensing UAV network that maximized the beam gain of the target signal between UAVs and MUs. To enhance the accuracy of the optimal beam vector, an artificial bee colony algorithm was used to obtain a suitable beam vector in [20]. However, beam alignment from UAVs to MUs cannot be achieved quickly due to the impact of the number of antennas on the complexity and time required to solve the optimization problem in a 3D beam-tracking scenario. In addition, the number of iterations of the optimization algorithms can also affect the beam alignment.

The beam vector is a crucial parameter for enhancing the accuracy of beam tracking in UAV-to-MU links. The time delay in finding the optimal beam vector significantly affects the accuracy of the beams. In addition, pilot overhead for channel estimation leads to energy consumption during both codebook-based and beam vector-optimized beam-tracking algorithm. To address these challenges, several studies have focused on angle of departure (AoD) and angle of arrival (AoA) in calculating beam vectors and proposed angle-aware predictive beam tracking based on localization. These algorithms enable the construction of a efficient beam-tracking mechanism without the need for pilot overhead between UAVs and MUs for channel estimation.

In [21], a long short-term memory-based recurrent neural network (LNet) was designed to predict the location of UAVs and calculate the corresponding angles. In [22], the UAV motion was viewed as a linear motion, and a modified least squares search was used to obtain the spatial angle from UAV to BS, thereby achieving beam tracking in the BS-to-UAV links. In [23], Kalman filtering was used to predict the spatial angle between the UAV and BS. This approach provided less training overhead and high beam alignment accuracy for beam tracking between BS and UAV. In [24], GPR was utilized to predict the locations of UAVs. However, the time delay between BS and UAVs impacts the accuracy of beam tracking from UAVs to MUs. To mitigate the effect of predictive angle errors on beam alignment, an algorithm for wide beam construction was proposed in [14]. However, this approach reduces the beam gain received at MUs. Various models such as SVM, Kalman filter, and Bayesian perspective were used to predict spatial angles of MUs by BS [4], [25], [26]. These algorithms always used historical trajectories to train the model. However, the trained model cannot accurately predict the UAV trajectory due to significant yet random impacts caused by the wind and other environmental factors. Nevertheless,

TABLE I
COMPARISONS OF THE EXISTING METHODS AND THIS WORK

Methods	Reference	UAV cooperation	Spatial angle prediction	Dynamic beam reconstruction	Real-time communication	Low complexity
Codebook based beam-tracking algorithms	[13]	×	×	✓	×	✓
	[15]	×	×	×	×	✓
	[17]	×	×	×	×	✓
Beam vector optimized with optimization algorithms	[18]	×	×	×	×	×
	[19]	✓	×	×	×	×
	[20]	×	×	×	×	×
Angle-aware beam-tracking algorithms	[21]	×	✓	×	✓	✓
	[23]	×	✓	×	✓	✓
	[14]	×	✓	×	✓	✓
BAB-AR	This work	✓	✓	✓	✓	✓

the dynamic time interval for beam reconstruction has been overlooked, which results in an interruption in communication between the target MU and BS when the MU moves rapidly.

III. SYSTEM MODEL

A. Network model

The beam-tracking system in this study is comprised of beam-tracking among UAV-BSs and UAVs to MUs. Each UAV can follow its own pre-set trajectory. For simplify, all UAVs are assumed to be on the same plane, and MUs are considered as cars that are always in motion. As illustrated in Fig.1, the flight area of UAV-BSs is defined as $[(0, 0), (x_{max}, y_{max})]$, where k position-known assisted UAVs (A-UAV) and m position-unknown assisted UAVs (U-UAV) at altitude h as UAV-BSs are assumed to provide the service of beam tracking to MUs. The A-UAVs, which are randomly distributed in the area, are equipped with high-precision GPS and $N = N_{ULA}$ uniform line array (ULA). The U-UAVs are equipped with $N = N_x \times N_y$ uniform planar array (UPA) to provide beam-tracking for MUs [13]. They also have a single antenna to receive information from A-UAVs.

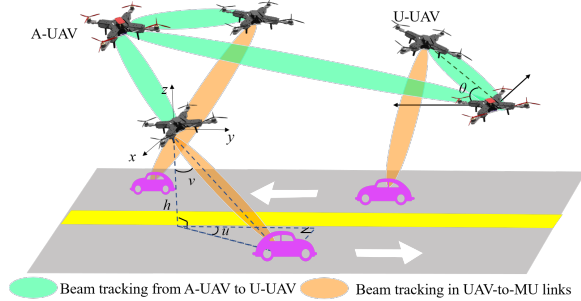


Fig. 1. Communication model between UAVs and MUs.

B. Channel model

The mmWave channel used in this study is typically sparse in space, and the AoD and AoA change as UAVs and MUs

move [3], [26]. To achieve adaptive beam tracking among UAV-BSs, the position unknown U-UAV sends reference signals such as demodulation reference signals (DMRS) to locate themselves [22], [27]. The proposed scenario has two beamforming approaches: 2D beamforming among UAV-BSs and 3D beamforming towards MUs.

1) *2D beamforming from A-UAVs to U-UAVs*: As UAV-BSs, the locations of the A-UAV_k and the U-UAV_i are denoted as (x_k, y_k) and (x_i, y_i) , respectively, under a 2D coordinate system. Then the spatial angle $\theta_{i,k}$ of the A-UAV_k relative to the U-UAV_i can be expressed as follows:

$$\theta_{i,k} = \arctan \frac{y_i - y_k}{x_i - x_k} \quad (1)$$

The direction vector $a_{i,k} \in \mathbb{C}^{N_{ULA} \times 1}$ of the reference signal received at the A-UAV_k can be expressed as follows:

$$a_{i,k} = \left[1, e^{-j \cos \theta_{i,k}}, \dots, e^{-(N_{ULA}-1)j \cos \theta_{i,k}} \right] \quad (2)$$

In this study, the Rayleigh fading model, which is usually used for LoS paths, is used between the A-UAV_k and the U-UAV_i [14], [21]. Then the channel matrix $H_{i,k}$ between the A-UAV_k and the U-UAV_i can be expressed as follows:

$$H_{i,k} = \frac{c\rho}{4\pi f_c d_{i,k}} \quad (3)$$

where f_c is the operating frequency, c is the speed of light, ρ is the channel fading parameter, and $d_{i,k}$ represents the straight-line distance between the A-UAV_k and the U-UAV_i. $d_{i,k}$ can be calculated as follows:

$$d_{i,k} = \sqrt{(x_i - x_k)^2 + (y_i - y_k)^2} \quad (4)$$

The received signal at the A-UAV_k equipped with a ULA can be expressed as follows:

$$\begin{aligned} r_{i,k} &= \rho H_{i,k} a_{i,k}^H s_{i,k} + n \\ &= \frac{c\rho}{4\pi f_c d_{i,k}} a_{i,k}^H s + n \end{aligned} \quad (5)$$

Let $s_{i,k}$ denote the reference signal sent from the U-UAV_i to the A-UAV_k, and $n_0 \sim \mathcal{CN}(0, \sigma^2)$ is Gaussian white noise,

where σ^2 set as 1. The signal received at U-UAV_i from A-UAV_k can be expressed as follows:

$$\begin{aligned} r_{k,i} &= \sqrt{N_{ULA}\rho} w_{i,k} H_{i,k} a_{k,i}^H s_{i,k} + n \\ &= \frac{\sqrt{N_{ULAC}\rho}}{4\pi f_c d_{i,k}} w_{i,k} a_{k,i}^H s + n \end{aligned} \quad (6)$$

Given that the UAVs are in the same plane, the spatial angle from U-UAV_i to A-UAV_k is equal to the spatial angle from A-UAV_k to U-UAV_i, and the direction vector $a_{i,k}$ is equal to $a_{k,i}$ as shown in Eq. (2). In addition, $s_{k,i}$ in Eq. (6) denotes the signal sent from the A-UAV_k to the U-UAV_i, and $w_{i,k}$ is the beam vector from the A-UAV_k to the U-UAV_i, which can be expressed as follows:

$$w_{i,k} = \frac{1}{\sqrt{N_{ULA}}} 1, e^{-j \cos \hat{\theta}_{i,k}}, \dots, e^{-(M-1)j \cos \hat{\theta}_{i,k}} \quad (7)$$

where $\hat{\theta}_{i,k}$ is the optimized angle from U-UAV_i to A-UAV_k which can be calculated as follows:

$$\hat{\theta}_{i,k} = \arctan \frac{\hat{y}_i - y_k}{\hat{x}_i - x_k} \quad (8)$$

The calculation of the optimized location of U-UAV_i (\hat{x}_i, \hat{y}_i) is introduced in Section IV.

2) *3D beamforming from U-UAV to the target MU*: The location coordinate of the target MU_l is $(x_l, y_l, 0)$ and the U-UAV_i is (x_i, y_i, h) under a 3D coordinate system as shown in Fig. 1. Thus, the distance between the MU_l and the U-UAV_i can be expressed as follows:

$$d_l = \sqrt{(x_l - x_i)^2 + (y_l - y_i)^2 + h^2} \quad (9)$$

The azimuth and elevation angles u_l and v_l from the MU_l to the U-UAV_i can be calculated by the locations of MU_l as follows:

$$u_l = \arctan \frac{y_l - y_i}{x_l - x_i} \quad (10)$$

$$v_l = \arctan \frac{\sqrt{(y_l - y_i)^2 + (x_l - x_i)^2}}{h} \quad (11)$$

After the A-UAV_k predicts the spatial angle of the MU_l and transmits data containing the locations of U-UAVs and MU_l to the U-UAV_i, the U-UAV_i equipped with the $N_x \times N_y$ UPA can provide beam-tracking to the MU_l. Additionally, the channel matrix H_l between the U-UAV_i and the MU_l can be expressed as follows:

$$H_l = \frac{c\rho_l}{4\pi f_c d_l} \quad (12)$$

where ρ_l is the channel fading between the U-UAV_i, the MU_l, d_l denotes the distance between the U-UAV_i and the MU_l, and the signal direction vector $a_l(u_l, v_l)$ emitted from the U-UAV_i to the MU_l can be denoted as follows:

$$a_l(u_l, v_l) = (1, e^{j2\pi c/f_c(\cos v_l + \sin v_l) \sin u_l}, \dots, e^{j2\pi c/f_c((N_x-1) \cos v_l + (N_y-1) \sin v_l) \sin u_l}) \quad (13)$$

Thus the signal received by the MU_l can be expressed as follows:

$$\begin{aligned} r_{i,l} &= \sqrt{N_x \times N_y} w_l(\hat{u}_l, \hat{v}_l) H_l a_l(u_l, v_l)^H + n \\ &= w_l(\hat{u}_l, \hat{v}_l) \frac{\sqrt{N_x \times N_y} c\rho_l}{4\pi f_c d_l} a_l(u_l, v_l)^H + n \end{aligned} \quad (14)$$

where w_l is the beam vector from the U-UAV_i to the MU_l, which can be denoted as follows:

$$\begin{aligned} w_l(\hat{u}_l, \hat{v}_l) &= \frac{1}{\sqrt{N_x \times N_y}} (1, e^{j2\pi c/f_c(\cos \hat{v}_l + \sin \hat{v}_l) \sin \hat{u}_l}, \\ &\dots, e^{j2\pi c/f_c((N_x-1) \cos \hat{v}_l + (N_y-1) \sin \hat{v}_l) \sin \hat{u}_l}) \end{aligned} \quad (15)$$

where \hat{u}_l and \hat{v}_l are the predicted azimuth and elevation angles from the MU_l to the U-UAV_i. Moreover, the half power beam width (HPBW) of the beam in azimuth plane and elevation plane can be calculated as follows:

$$\theta_u(u, v) = \frac{1}{\cos u \sqrt{\Delta\theta_u^{-2} \cos^2 v + \Delta\theta_v^{-2} \sin^2 v}} \quad (16)$$

$$\theta_v(u, v) = \frac{1}{\sqrt{\Delta\theta_u^{-2} \sin^2 v + \Delta\theta_v^{-2} \cos^2 v}} \quad (17)$$

where $\Delta\theta_u$ and $\Delta\theta_v$ are the HPBW of the beam constructed by linear array with N_x and N_y antennas, respectively, the calculation can be expressed as follows:

$$\Delta\theta_u = \frac{\lambda \times 2}{N_x} \quad (18)$$

$$\Delta\theta_v = \frac{\lambda \times 2}{N_y} \quad (19)$$

IV. BI-DIRECTIONAL ANGLE-AWARE BEAM-TRACKING WITH ADAPTIVE BEAM RECONSTRUCTION ALGORITHM

Existing angle-aware beam-tracking algorithms have been developed for scenarios involving the communication between BS and MUs or BS and UAVs [14] [21]–[27]. However, these algorithms fail to address the fixed height of the BS, which results in a lack of LoS links. The time delay in transmitting signals from the BS to UAVs also affects the accuracy of UAV localization, and existing algorithms struggle to maintain stability across different movement patterns of UAVs. Consequently, the accuracy of beam tracking from UAVs to MUs remains unsatisfactory. In addition, the time interval for predicting the angle used during beam reconstruction for high-speed MUs is not considered. To address these limitations, this study proposes a bi-directional angle-aware beam-tracking with adaptive beam reconstruction (BAB-AR) algorithm.

The communication cycle in BAB-AR is divided into two parts: angle-aware beam-tracking within UAV-BSs and beam tracking from UAVs to MUs. As Fig. 2 shows, the two processes of A-UAVs, localization for U-UAVs and collection for the historical trajectory of the target MU, run in parallel. During U-UAV localization phase, GDCSA is proposed to accurately locate U-UAVs without GPS for fast convergence. Once the localization of U-UAVs is finished, the historical spatial angles from MU to U-UAV can be obtained using Eq. (10) and Eq. (11), and the GPR model can be trained by A-UAV for the target MU. As the model and predicted locations of U-UAV are updated, beam tracking within the UAV-BSs can be carried out as described in Section III. B. Furthermore, the real-time information, such as the optimized U-UAVs locations and the predicted angles from the target MU to U-UAV, can be transmitted from A-UAVs to U-UAVs.

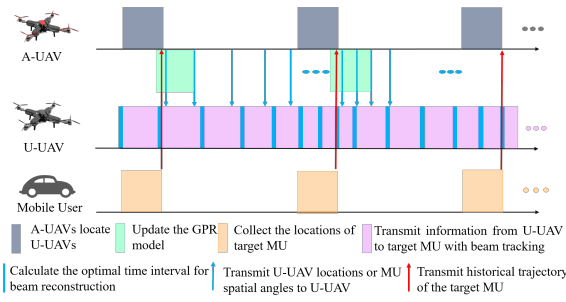


Fig. 2. Time frame of the BAB-AR algorithm.

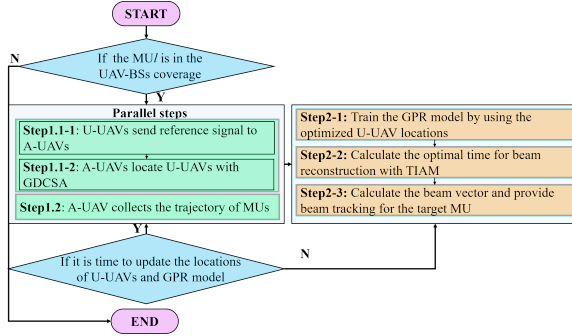


Fig. 3. Flow chart of BAB-AR algorithm.

During the communication between UAV and MU, the trained GPR model is used to predict the spatial angles from the MU_l to the $U-UAV_i$ at time $t_{n-1} + \Delta t_n^*$, where Δt_n^* is the dynamic time interval calculated by TIAM for beam reconstruction. With the predicted locations of $U-UAV_i$ and spatial angle of MU_l , the $U-UAV_i$ can provide timely beam tracking for the high-speed MU_l . In this phase, only location information needs to be collected, thus, the pilot overhead caused by channel estimation can be decreased [21]. In addition, A-UAV updates the locations of U-UAVs every t_{check} , and the efficiency of the model is checked with the new trajectory of the target MU. The flow chart of BAB-AR is shown in Fig. 3.

A. Localization of UAV-BSs via the proposed GDCSA

The accurate localization of UAV-BSs using GPS for beam construction is costly. Moreover, existing angle-aware beam-tracking algorithms for the UAV-BSs usually require the historical trajectory of UAVs to perform location prediction. However, the locations of UAVs are always affected by environmental factors such as wind, and the historical trajectory information may not be accurate when training a model to predict UAV location. To address this issue, the GDCSA is designed with low computing complexity to cooperatively locate U-UAVs by A-UAVs without the historical trajectory data. A-UAVs can calculate the position of U-UAV collaboratively by utilizing the signal transmitted from the U-UAV to the A-UAVs. Therefore, the accuracy of the predictive location cannot be affected by the moving patterns or the shaking of UAV, since the localization process is independent of the U-UAV historical trajectory.

1) *GDCSA*: Crow search algorithm (CSA) is a swarm intelligence optimization algorithm with fast convergence [28]. In CSA, each crow's position in the search space represents a feasible solution, and all crows gradually explore the search space by leveraging the objective function's value as a reference. The iterative process eventually leads to a global optimal solution.

In CSA, crow i randomly selects a crow j from the population as the learning target at each iteration, and then the location of crow i is updated as follows:

$$X_i^{t+1} = \begin{cases} X_i^t + r_i \times fl_i^t \times |m_i^t - X_i^t|, & r_i \geq AP_i^t \\ \text{a random position,} & \text{otherwise} \end{cases} \quad (20)$$

where, AP_i^t denotes the probability that the crow i found the optimal crow at the t iteration. fl_i^t denotes the flight distance of the crow i at the t iteration, and r_i is a random number between 0 and 1. One limitation of the original CSA is that the initial positions of crows are generated randomly, which can lead to an uneven distribution of solutions in the search space. Moreover, in the original CSA, the value of AP_i^t remains constant throughout the algorithm, which can slow down the convergence speed.

A GDCSA is proposed to increase the global search ability of crows and improve the optimization accuracy. In this approach, the optimal point set is used to initialize the crows, which can be calculated using Eq. (21). The crows then disperse evenly across the search space, as depicted by the stars in Fig. 4. Thus, the global search ability of the crows is enhanced, which leads to superior optimization results [29].

$$P_n(k) = \{(\{r_1^{(n)} \times k\}, \{r_2^{(n)} \times k\}, \dots, \{r_s^{(n)} \times k\}), 1 \leq k \leq n\} \quad (21)$$

where r_i is set as follows:

$$r_i = \left\{ 2 \cos \frac{2\pi i}{p}, 1 \leq i \leq s \right\} \quad (22)$$

where s is the number of points, and p is the smallest prime number which satisfies the condition as follows:

$$\frac{p-3}{2} \geq s \quad (23)$$

A dynamic parameter AP_i^t adapted to the number of iterations is likewise designed to enhance the rate of convergence.

$$AP_i^t = \beta \left(\frac{iter_max - t}{iter_max} \right)^2 \quad (24)$$

where $iter_max$ is the initial maximum iteration number of the algorithm, and t is the current number of iterations. According to Eq. (24), the initial value of AP is substantial, but it gradually decreases as the iterations continue.

2) *U-UAVs localization based on GDCSA and beam construction*: In this section, the GDCSA is used to locate U-UAVs by A-UAVs. The scenario involves k A-UAVs and m U-UAVs functioning as UAV-BSs. Based on the received signal at A-UAVs from U-UAVs, A-UAVs locate U-UAVs with GDCSA cooperatively. During the localization phase, A-UAVs with known locations communicate with each other through beam tracking. However, if U-UAVs A and B are symmetrical

where Radial Basis Function (RBF) is chosen as the kernel function to adapt the changes of the spatial angles u of the MU_l , which can be defined as follows:

$$K(T, T') = \exp\left(-\frac{\|T - T'\|^2}{2\sigma^2}\right) \quad (31)$$

The spatial angle $u[t_{n+1}]$ at t_{n+1} can be predicted when the value of $g_u(t)$ is t_{n+1} . Although the distribution of $g_u(t_{n+1})$ is unknown, the random variable consisting of $g_u(t_{n+1})$ and $Y = g_u(T)$ satisfies a Gaussian distribution as demonstrated in follows:

$$\begin{pmatrix} Y \\ g_u(t_{n+1}) \end{pmatrix} = N\left(\begin{pmatrix} \mu(T) \\ \mu(t_{n+1}) \end{pmatrix}, \begin{pmatrix} K(T, T) + \sigma_u^2 I & K(T, t_{n+1}) \\ K(t_{n+1}, T) & K(t_{n+1}, t_{n+1}) \end{pmatrix}\right) \quad (32)$$

The GPR model can calculate the posterior distribution of $g_u(t_{n+1})$, which can be expressed as follows:

$$P(f(T^*) | Y, X, X^*) = N\left(\mu^*, \sum^*\right) \quad (33)$$

where μ^* and \sum^* can be expressed as follows:

$$\mu^* = K(t_{n+1}, T) (K(T, T) + \sigma_u^2 I)^{-1} (Y - \mu(T)) + \mu(t_{n+1}) \quad (34)$$

$$\sum^* = K(t_{n+1}, t_{n+1}) - K(t_{n+1}, T) (K(T, T) + \sigma_u^2 I)^{-1} K(T, t_{n+1}) \quad (35)$$

where σ_u^2 represents the noise variance of the training data. Bringing the predictions \hat{u}_l, \hat{v}_l for the MU_l into Eq. (15), the beam vector for the link between the U-UAV $_i$ and the MU_l can be calculated as follows:

$$w(u_l, v_l) = (1, e^{j2\pi c/f_c(\cos \hat{v}_l + \sin \hat{v}_l) \sin \hat{u}_l}, \dots, e^{j2\pi c/f_c((N_x - 1) \cos \hat{\varphi}_l + (N_y - 1) \sin \hat{v}_l) \sin \hat{u}_l}) \quad (36)$$

Then the beam can be constructed from the U-UAV $_i$ to the MU_l . Meanwhile, the communication link can be established between UAV-BSs and MUs at time t_{n+1} .

C. Adaptive beam reconstruction with TIAM

The beam can be constructed by the U-UAV $_i$ for the MU_l once the angle is predicted by GPR. However, if the time interval Δt for beam reconstruction cannot adapt the movement of the MU_l , the MUs may move out of the limited HPBW of the constructed beam. As shown in Fig. 5, when the target MU moves out, the beam should be rebuilt to cover the moving MU. In addition, a shorter time interval Δt will result in frequent beam reconstruction, which leads to extra energy dissipation. Thus, a TIAM is proposed for the adaptive beam reconstruction during beam tracking from the U-UAV $_i$ to the MU_l , and the time interval Δt can be set dynamically according to the moving state of the MU_l . Then the beam will be reconstructed at $t_n + \Delta t_n$, where t_n represents the time of the last beam reconstruction. In addition, the moving state is determined by the angles predicted by GPR.

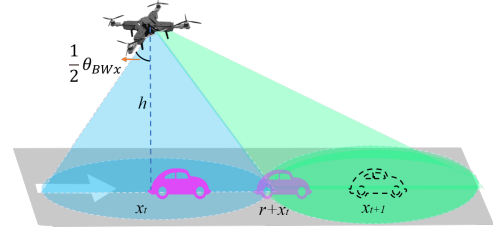


Fig. 5. Beam reconstruction with fixed time interval.

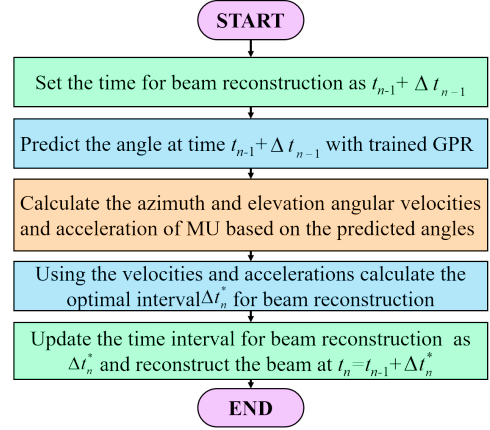


Fig. 6. Flow chart of the proposed TIAM.

As Fig. 6 shown, the time interval Δt_n for beam reconstruction is set as Δt_{n-1} at the beginning of TIAM, when $n = 0$, Δt_n is set as the time interval of the training data (MU_l 's trajectory). The movement of MU_l during the time interval Δt_n is modeled as uniformly accelerated motion as follows:

$$\Delta r_n = \omega_n + \frac{1}{2} \alpha_n \Delta t_n^2 \quad (37)$$

where Δr_n is the angle the MU_l moved during the time interval Δt_n . Δt_n means the time interval for beam reconstruction between time index t_n and t_{n+1} . ω_n is the angular velocity of the MU_l . In the 3D beamforming scenario, two angular velocities ω_{u_n} and ω_{v_n} can be calculated based on the prediction angles at time t_n and t_{n-1} as follows:

$$\omega_{u_n} = \frac{u_{n+1} - u_n}{\Delta t_n} \quad (38)$$

$$\omega_{v_n} = \frac{v_{n+1} - v_n}{\Delta t_n} \quad (39)$$

where $u_n, u_{n+1}, v_n, v_{n+1}$ are the spatial angles from MU_l to U-UAV $_i$ predicted by the trained GPR model at time t_n and $t_{n+1} = t_n + \Delta t_n$. If $n = 0$, the $u_n, u_{n-1}, v_n, v_{n-1}$ are the real-time spatial angles calculated by the collected locations of MU_l . Meanwhile, angular acceleration of the MU_l $\alpha_{u_n}, \alpha_{v_n}$ can be calculated based on angular velocities as follows:

$$\alpha_{u_n} = \frac{\omega_{u_{n+1}} - \omega_{u_n}}{\Delta t_n} \quad (40)$$

$$\alpha_{v_n} = \frac{\omega_{v_{n+1}} - \omega_{v_n}}{\Delta t_n} \quad (41)$$

Thus, the azimuth and elevation angular velocities and acceleration of MU_l can be calculated. Then, for the two different spatial angles, set Δr_n in Eq. (37) as HPBW θ_u and elevation plane HPBW θ_v of the beam, respectively, and take Eq. (16) and Eq. (17) into Eq. (37). The optimal value $\Delta t_n = \Delta t_n^*$ can be calculated as follows:

$$\Delta t_n^*(u_n, v_n, \omega_{u_n}, \omega_{v_n}, \alpha_{u_n}, \alpha_{v_n}) = \min(\Delta t_{u_n}, \Delta t_{v_n}) \quad (42)$$

where Δt_{u_n} and Δt_{v_n} can be calculated as follows:

$$\Delta t_{u_n} = \sqrt{2 \times \left(\frac{\theta_{u_n}}{2} - \omega_{u_n} \right) / \alpha_{u_n}} \quad (43)$$

$$\Delta t_{v_n} = \sqrt{2 \times \left(\frac{\theta_{v_n}}{2} - \omega_{v_n} \right) / \alpha_{v_n}} \quad (44)$$

Because the azimuth and elevation HPBW of the constructed beam are limited. Thus, the value of Δt_n is small when MU_l moves fast, and vice versa. MU_l can stay in the coverage area of the beam constructed by U-UAV, and the energy consumption for beam reconstruction can be decreased. The pseudo-code is listed in detail as below.

Algorithm 2 Angle-aware beam-tracking with adaptive beam reconstruction

Input: $u_{n-1}, v_{n-1}, u_n, v_n$ of MU_l , GPR models $model_u, model_v$ for u and v of MU_l , number of antennas $N_{UPA} = N_x \times N_y$, real-time t_s , time interval Δt

Output: The optimized time interval Δt_n^* for beam reconstruction

while t_s **do**

if t_s is time to collect data from the MU_l and one of the errors between predictive angles u, v and real angles u, v is bigger than σ_{check} **then**

 Rebuild the GPR model for u or v whose predictive error is over σ_{check}

end if

 Calculate the $\omega_{u_{n-1}}, \omega_{v_{n-1}}$, with $u_{n-1}, v_{n-1}, u_n, v_n$

 Calculate the HPBW with N_x, N_y, u_n, v_n

 Use $model_u$ and $model_v$ to predict u_{n+1}, v_{n+1} at $T_s + \Delta t$

 Calculate the $\omega_{u_n}, \omega_{v_n}$ with $u_n, v_n, u_{n+1}, v_{n+1}$

 Calculate the angular acceleration with $\omega_{u_{n-1}}, \omega_{v_{n-1}}, \omega_{u_n}, \omega_{v_n}$

 Calculate the optimal Δt_n^* with angular acceleration α_u, α_v , HPBW and $\omega_{u_n}, \omega_{v_n}$

 Update Δt as Δt_n^*

 Update T_s as $T_s + \Delta t$

 Update u_{n-1} as u_n, v_{n-1} as v_n

 Update u_n, v_n as $model_u, model_v$ predict at t_s

 Calculate the beam vector from the U-UAV $_i$ to the MU_l with u_n, v_n

 Build beam from the U-UAV $_i$ to the MU_l

end while

return The optimal result (\hat{x}, \hat{y}) as the location of U-UAV $_i$

D. Theoretical Analysis of the Proposed BAB-AR

Owing to building 3D beam tracking between UAV and MU, the computational complexity of the optimized beam vector algorithm is proportional to the number of antennas [19]. Thus, the complexity of the optimized function is $\mathcal{O}(N^{3.5})$, where N is the number of the UPA's antennas [18] [20]. Meanwhile, the optimal value of the beam vector is dependent on the number of iterations performed by the algorithm. Thus, the complexity of the beam vector-optimized method is $\mathcal{O}(N_{iter}N^{3.5})$, where N_{iter} denotes the number of iterations required for convergence.

In the proposed BAB-AR, a GPR algorithm is used to predict the angles of the target MU based on historical trajectory, which eliminates extra time for channel estimation in the 3D beam-tracking scenario. In addition, the trajectory information collection for the MU and U-UAVs localization are parallel process. Thus, the GPR model training can be completed once the U-UAV is located. The time required for model training can be ignored as the GPR model can be trained with minimal data in a short period. The total time consumption of BAB-AR is only dependent on the time taken by A-UAVs to locate U-UAVs using GDSCSA. Since GDSCSA's computation dimension is always two, the complexity of solving Eq. (25) is only relative to the dimension of $a_{i,k}$, which is N_{ULA} , and the complexity of the proposed BAB-AR is $\mathcal{O}(N_{ULA} \times N_{iter} \times N_{pop})$, where N_{pop} is the number of the initial populations.

The hybrid-codebook beam tracking algorithm has the lowest complexity $\mathcal{O}(N_c)$ among the aforementioned methods. The complexity of hybrid-codebook beam tracking algorithm is only dependent on the number of the fixed codebook N_c . However, it fails to provide high beam gain for MU_l .

V. EXPERIMENTS AND DISCUSSIONS

This section verifies the robustness of the proposed BAB-AR algorithm against three baseline algorithms: hybrid codebook-based beam-tracking [30], beam vector-optimized beam-tracking algorithm [19], and angle-aware beam-tracking algorithm without data processing based on GPR [14]. This study considers UAV-BSs with a height of 100m distributed in an area of $[(0, 0), (150, 150)]$. The number of antennas for U-UAVs is set to 16×16 , while the number of antennas for A-UAVs is set to 16. During the experiments, k is set to 2, and the coordinates of A-UAVs are (0, 0), (50, 50), respectively. In the phase of collecting MU_l 's trajectory, A-UAVs collect location information from the MU_l every Δt_n . The prediction model is rebuilt at each t_{check} . The meaning of the variables used in this section is listed in Table II.

A. Accuracy analysis of angle prediction with BAB-AR algorithm

1) *Angle prediction of UAV-BSs:* The proposed GDSCSA is used by A-UAVs to locate U-UAVs in a cooperative manner. Table III demonstrates that the optimized results obtained by three distinct algorithms. The proposed GDSCSA exhibits superior accuracy over both CSA and PSO algorithms. Furthermore, the GDSCSA algorithm requires less running time to

TABLE II
 VARIABLES IN EXPERIMENTS

Parameter	Value	Description
h	100	Drone flight altitude
$N_x \times N_y$	16×16	Specifications of the U-UAV equipped with a surface array
N_{ULA}	16	Specifications for drones equipped with line arrays
k	2	Number of A-UAVs
(x_i, y_i)	(x_i, y_i)	Location of the U-UAV $_i$ within the flight area
u_i	u_i	The angle of U-UAV $_i$ calculated based on (x_i, y_i) within the flight area
$\theta_{i,k}$	$\theta_{i,k}$	The spatial angle from the U-UAV $_i$ to the A-UAV $_k$
(u_l, v_l)	(u_l, v_l)	The spatial angle from the MU $_l$ to the U-UAV $_i$
(\hat{x}_i, \hat{y}_i)	(\hat{x}_i, \hat{y}_i)	The predicted location of the resulting the U-UAV $_i$ within the flight area
\hat{u}_i	\hat{u}_i	The angle of U-UAV $_i$ calculated based on (\hat{x}_i, \hat{y}_i) within the flight area
$\hat{\theta}_{i,k}$	$\hat{\theta}_{i,k}$	The predicted spatial angle from the U-UAV $_i$ to the A-UAV $_k$
(\hat{u}_l, \hat{v}_l)	(\hat{u}_l, \hat{v}_l)	The predicted spatial angle from the MU $_l$ to the U-UAV $_i$
n	when $\Delta t_n = 0.1s, n \in [0, 50]$; when $\Delta t_n = 0.01s, n \in [0, 500]$;	Number of the time index in a trajectory
t_n	$n \times \Delta t_n$	Time index during the experiment
Δt_n	0.1s	Time interval for the UAV $_i$ to collect the location information of the MU $_l$
Δt_n^*	Dynamical time interval and the initial value is 0.1s	Time interval for predicting the spatial angle of the MU $_l$
t_{check}	3s	Time interval for checking if GPR model should be rebuilt
σ_{check}	0.05π	Threshold value for checking if GPR model should be rebuilt

 TABLE III
 COMPARISON OF THE CONVERGENCE SPEED

Algorithm	Value of fitness	Running time/s
GDCSA	2.81	1.09
CSA	10.95	1.38
PSO	80.84	1.13

obtain the optimal result in comparison to the original CSA algorithm.

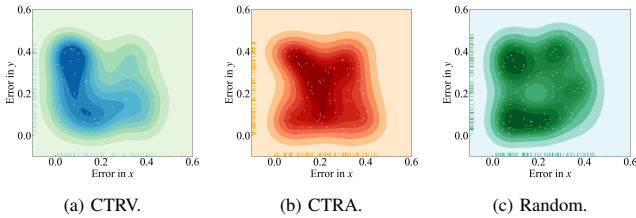
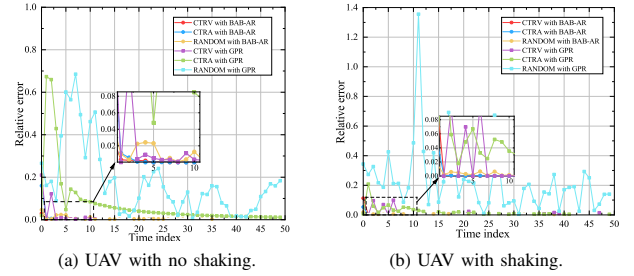

 Fig. 7. Error between (\hat{x}_i, \hat{y}_i) and (x_i, y_i) in different moving patterns.

Fig. 7 shows the prediction error of the target U-UAV from time index t_0 to t_{50} in different moving patterns, including constant turn rate and velocity (CTRV), constant turn rate and acceleration (CTRA), and random wandering. The colors of the regions represent the prediction error distribution between (\hat{x}_i, \hat{y}_i) predicted by GDCSA and real (x_i, y_i) , and the boundary of the regions represent the range of error values. Specifically, the darker color of the region represents the denser distribution of error values. As can be seen, the proposed GDCSA can precisely locate U-UAVs while the errors between (\hat{x}_i, \hat{y}_i) and (x_i, y_i) are all within 0.5 m in different moving patterns, which means that the performance of GDCSA is stable in different moving patterns. The reason is that the localization process in GDCSA is not dependent on the trajectory of U-UAVs, but rather on the strength of the reference signal received at A-UAVs.

Based on the optimized locations, the spatial angles from the U-UAV $_i$ to the A-UAV $_k$ can be calculated. Fig. 8 shows the relative errors between u_i and \hat{u}_i estimated by GDCSA and the


 Fig. 8. Relative errors between $\theta_{i,k}$, and $\hat{\theta}_{i,k}$ in different moving patterns.

GPR algorithm proposed in [14]. CTRV, CTRA, and random wandering moving patterns are considered in this experiment. In Fig. 8(a), the UAV moves without any shaking, while in Fig. 8(b), the UAV's locations are fluctuated within a 50m radius by the UAV shaking. As shown in Fig. 8(a), the angle relative error of the BAB-AR algorithm is less than 0.2 under different motion patterns. However, the angle relative error of the algorithm [14] is less than 0.2 only when the UAVs move under the CTRV moving pattern. In random moving pattern, its relative error is 0.6. In brief, the GDCSA can predict spatial angles with high accuracy under various UAV moving patterns. Meanwhile, Fig. 8(b) shows that the relative error in predictive angle calculated by GPR has obvious fluctuation due to the influence of shaking, as the historical trajectory information is used for spatial angle prediction. However, the accuracy of the predictive angle which is calculated by the predictive location cannot be affected by UAV shaking, and the error caused by GDCSA maintains a value less than 0.2.

In addition, the SNR at different U-UAVs under different moving patterns is also used to evaluate the performance of GDCSA. The SNR of the signal received at U-UAV $_i$ can be calculated as follows:

$$SNR = \frac{p_{k,i}|r_{k,i}|^2}{\sigma^2} \quad (45)$$

where $p_{k,i}$ is the transit power from A-UAV $_k$ to U-UAV $_i$, which is set as 20 dBm and the noise power is set as -100

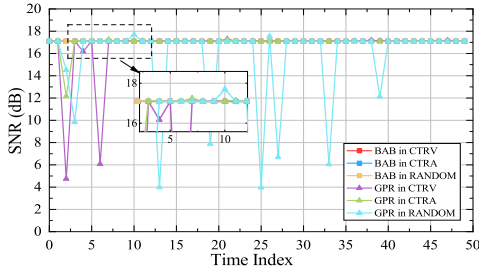


Fig. 9. SNR under different moving patterns.

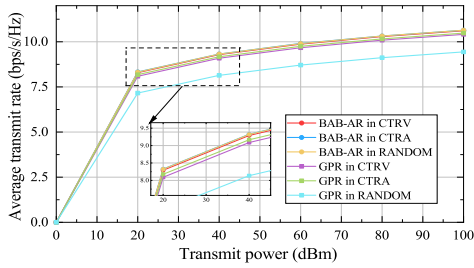


Fig. 10. Average rate under different transmit power.

dBm. Meanwhile, $r_{k,i}$ is the signal received at U-UAV $_i$ from A-UAV $_k$ as expressed in Eq. (6). As shown in Fig. 9, the shaking of UAVs does not affect the beam alignment, and high SNR can be maintained under different moving patterns by GDCSA. Because the location prediction of the proposed GDCSA is calculated based on the received signal strength of A-UAV. However, the angle prediction errors affect the beam alignment among U-UAVs in GPR.

Besides, the transmission rate, which can be expressed as Eq. (46) can also be improved with a high SNR:

$$\text{Rate} = \log_2(1 + \text{SNR}) \quad (46)$$

Fig. 10 shows that the average data transmission rate at U-UAVs with GDCSA is capable of achieving data transmission among UAV-BSs with high efficiency.

2) *Angle prediction of the target MU*: During the beam tracking phase between UAV and MUs, a trained GPR model is used to predict the spatial angle of the target MU $_l$. As illustrated in Fig. 11, predictive errors between (u_l, v_l) and (\hat{u}_l, \hat{v}_l) are presented under CTRV and CTRA moving patterns with $\Delta t = 0.1s$, respectively. The GPR without data processing exhibits instability. Nevertheless, the BAB-AR algorithm demonstrates an error margin of 0.025 or less under each moving pattern. The high accuracy of spatial angles prediction ensures the maintenance of high beam gain, as discussed in Section V.B. In Fig. 12, the real vehicle trajectory data¹ is used to verify the accuracy of the BAB-AR algorithm by comparing with other algorithms. The vehicle trajectory data was collected by Federal Highway Administration from a specified freeway segments in the USA. As shown in Fig. 12, BAB-AR can accurately predict the angles of MU. The

¹The simulation data of trajectory of GU is from “https://data.transportation.gov”

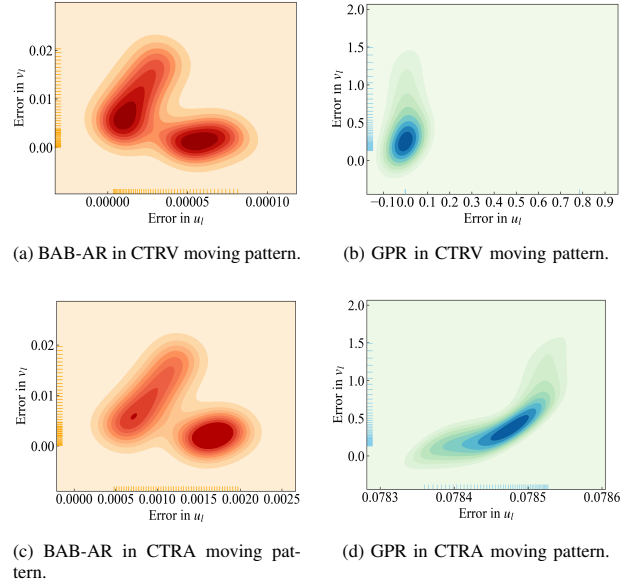
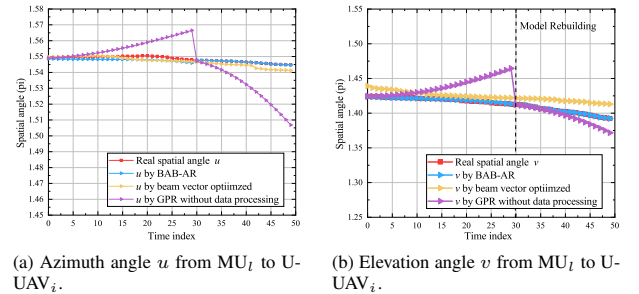

 Fig. 11. Errors between (u_l, v_l) and in the CTRA moving pattern.


Fig. 12. Angle prediction using different algorithms.

error between u_l and \hat{u}_l estimated by BAB-AR, beam vector optimized algorithm [19] and the angle predictive beam tracking algorithm based on GPR [14] are 0.1146° , 0.5675° , and 0.0114° , respectively. Similarly, the error between v_l and \hat{v}_l are 0.1547° , 0.6535° , and 0.6477° , respectively. The proposed BAB-AR algorithm has Superior accuracy than the GPR algorithm without data processing [14]. However, the alignment angle of the beam vector-optimized algorithm [19] satisfies accuracy requirements only when the spatial angle changes slowly as shown in Fig. 12(a). Because the beam tracking between UAV and MU is 3D beam-tracking channel, which takes more time for the beam vector-optimized algorithm [19] to compute the optimal beam vector.

In BAB-AR, the trajectory used for training the GPR model should adapt to the movement of the MU $_l$ in time. In this experiment, the update frequency of the GPR model t_{check} is set to 3s, and the error threshold σ_{check} between predictions and real data is set to 0.05π . In Fig. 12, the BAB-AR model is not rebuilt for azimuth angle u , but the model for elevation angle v is rebuilt at time index 30.

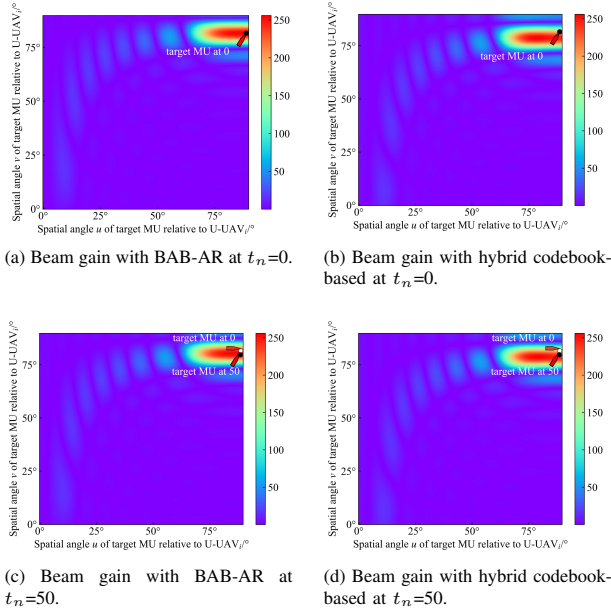


Fig. 13. Beam gain heat map.

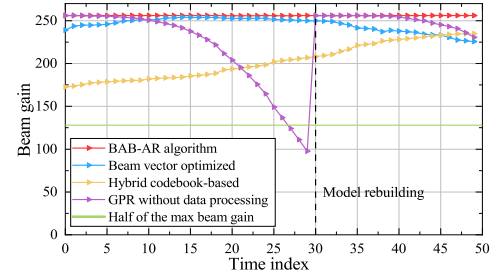
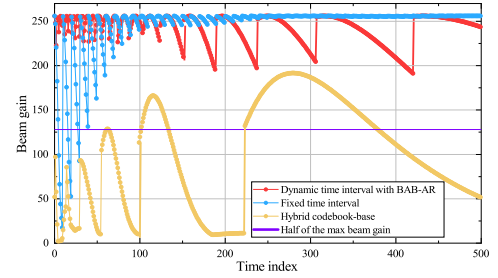
B. Comparison of beam gain at MU

In this experiment, the beam gain at the target MU can be calculated as follows:

$$G_{GU} = \sqrt{N_x \times N_y} w_l \cdot H \cdot a_l^H \quad (47)$$

The beam gain of the hybrid codebook-based beam-tracking algorithm [30] and BAB-AR algorithm at $t_n = 0$ and $t_n = 50$ are shown in Fig. 13, respectively. The maximum beam gain region is highlighted in red, while regions with decreasing beam gain are colored green and purple. At $t_n = 0$, the MU_l is located at the edge of the beam constructed by the hybrid codebook-based approach, which results in a green-colored region with a beam gain value of 172.57. At $t_n = 50$, the MU_l has moved to a region aligned with one of the constructed codebooks, which causes the color of region to change to red, and the beam gain value is increased to 234.78. In contrast, for BAB-AR, regions surrounding the MU_l are colored red at the $t_n = 0$ and $t_n = 50$, with beam gain value of 255.88 and 255.65, respectively. Thus, BAB-AR can construct an optimal beam for the MU_l promptly.

The beam gain of different algorithms with the real trajectory of MU is simulated as shown in Fig. 14. At $t_{check} = 3s$, the GPR model is rebuilt when $t_n = 30$. The beam gain of [19] is lower than that of other algorithms as the trajectory changes rapidly after $t_n = 30$. With the beam-tracking algorithm [30], the beam gain remains substantial only when the MU_l's location aligns with the coverage area of the constructed beam. The predictive accuracy of the GPR algorithm without data processing is inferior to that of the BAB-AR algorithm. The beam gain of the BAB-AR algorithm received at the MU_l is improved by approximately 5.52%, 21.58%, and 4.51% compared to those achieved by the beam vector optimized algorithm [19], hybrid codebook-based beam-tracking algorithm [30], and the angle-predictive beam tracking realized by GPR without data processing [14].


 Fig. 14. Beam gain at the MU_l per $\Delta t = 0.1s$ with different algorithms.

 Fig. 15. Beam gain received at the MU_l per $\Delta t = 0.01s$ with different algorithms.

C. Importance of dynamic beam reconstruction

The importance of dynamic beam reconstruction is shown in Fig. 15. A CTRA moving pattern with a time interval of $\Delta t = 0.01s$ is simulated. The time interval for beam reconstruction is determined by TIAM to cover the target MU within the HPBW of the beam, which can be calculated using Eq. (16) and Eq. (17). In these equations, the parameter λ is set as 0.886. When the target MU_l moves rapidly, such as between time index 0 and 100, the beam reconstruction with fixed time interval $\Delta t = 0.1s$ cannot adapt to the MU_l's motion, resulting in low beam gain that is insufficient for data transmission. With a fixed time interval, beam reconstruction occurs frequently after time index 100, and the decline in the beam gain is not obvious. For the hybrid codebook beam-tracking algorithm, high beam gain fails to meet transmission requirements when the MU_l moves quickly due to the fixed beam vector. However, the BAB-AR algorithm can reconstruct the beam when the MU_l moves away from the HPBW of the constructed beam. When the movement of MU_l is slow, the beam gain at the MU_l with BAB-AR is superior to the half of the maximum beam gain, and the frequency of beam reconstruction can be reduced with an adaptive beam reconstruction interval calculated by TIAM.

The energy efficiency (EE) of the above three mentioned algorithms under different MU movement speed is compared, and the EE at MU_l can be calculated as follows:

$$EE_l = \frac{Rate_l}{p_{i,l} + N_{RF}P_{RF} + N_x N_y P_{PS} + P_{BB}} \quad (48)$$

where P_{PS} is the power consumption of each phase shifter, P_{RF} is the power consumed by each RF chain, N_{RF} is the number of RF chains, and P_{BB} is the power consumption of

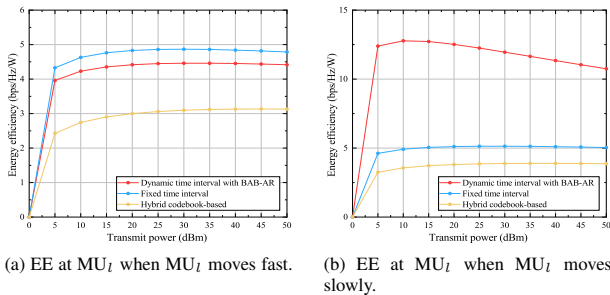


Fig. 16. Energy efficiency (EE) under different transmit power.

the baseband. In addition, the rate at MU_l can be calculated as follows:

$$Rate_l = \log_2(1 + SNR_l) \quad (49)$$

The growth trend of EE remains stable as the transmit power increases, as shown in Fig. 16. Because the transmit power rises as the impact of the total power consumption increase according Eq. (48). In this experiment, it is assumed that $P_{PS} = 40$ mW, $P_{RF} = 300$ mW, $N_{RF} = 1$, and $P_{BB} = 200$ mW [20]. As shown in Fig. 16(a), the EE of BAB-AR is lower compared to the fixed time interval mode when MU_l moves fast, because the frequent beam reconstruction consume much power. However, the beam gain at MU_l under the fixed time interval mode may not meet the required communication quality, as Fig. 15 shown. When MU_l moves slowly, as shown in Fig. 16(b), the EE of BAB-AR at MU_l improves significantly by up to 136.46% and 215.99% compared to that of the fixed time interval mode and hybrid-codebook algorithm, respectively. Because BAB-AR algorithm not only ensures that the beam gain remains at half of the maximum beam gain that the antenna can provide, but also reduces the number of beam reconstruction when the target MU_l moves slowly.

The average transmit rate at MU_l is evaluated under different transmit power level and speed, and the noise power is set as -100 dBm. The hybrid codebook's average transmit rate is not high enough due to the low beam gain at MU_l . In addition, when MU_l moves fast as shown in Fig. 17(a), the average transmit rate of BAB-AR is improved by up to 5.21% and 67.63% compared to that of the fixed time interval mode and hybrid-codebook algorithm. Because the beam in BAB-AR can be reconstructed according to the movement of the MU_l and cover the MU_l with HPBW. When MU_l moves slowly as shown in Fig. 17(b), the BAB-AR reconstructs beam only once, but the fixed time interval mode reconstructs beam 10 times. However, the difference in average transmit rate between BAB-AR and fixed time interval mode is less than 0.5.

D. Limitation of the BAB-AR algorithm

The time for constructing the optimal beams has a significant impact on the effectiveness of the algorithm in real scenarios. In particular, the shorter the time consumed, the more beneficial for real-time beam alignment in high-mobility

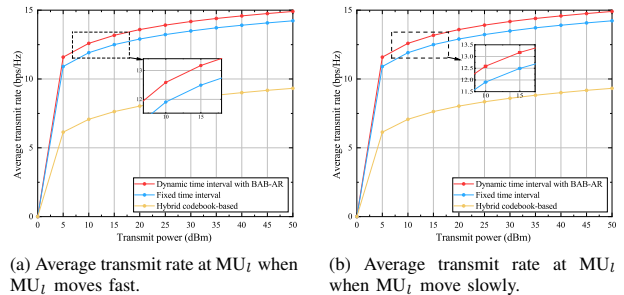


Fig. 17. Average transmit rate under different transmit power.

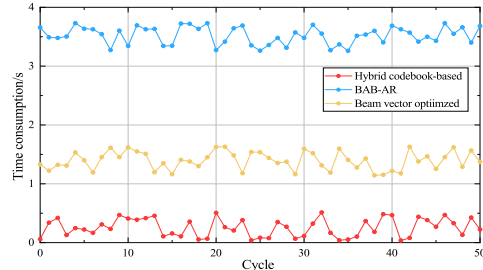


Fig. 18. Running time of different algorithms.

scenarios. The complexity of the codebook beam-tracking algorithm [30] is $\mathcal{O}(N_c)$, where N_c is the number of designed codebook, while the complexity of the beam vector-optimized algorithm [19] and the proposed BAB-AR are $\mathcal{O}(N_{iter} \times N_{3.5})$ and $\mathcal{O}(N_{ULA} \times N_{iter} \times N_{pop})$, respectively, as mentioned in Section IV. In Fig. 18, we set the number of antennas as 16×16 , and compare the time consumption of BAB-AR algorithm, beam vector-optimized beam-tracking algorithm [19], and hybrid codebook-based algorithm [30] in each cycle. BAB-AR consumes more time than that of the codebook-based beam alignment algorithm. However, compared to the algorithm proposed in [19], the proposed BAB-AR algorithm can reduce the time consumption by 44.89%.

The impact of the numbers of UPA's antennas on the time consumption of different algorithms is shown in Fig. 19. As the number of antennas increase, so does the time required to obtain the optimal beam vector. The performance of BAB-AR is better than that of the beam vector optimized [19], and its time consumption does not increase obviously with the number of antennas. However, BAB-AR still has a higher time consumption than that of the hybrid codebook-based algorithm. Despite reducing the dimension of the optimized problem, BAB-AR's time consumption is proportional to the number of ULA antennas equipped on A-UAV, the number of iterations and the initial population, resulting in extra time for beam selection compared to that of the hybrid-codebook algorithm.

We also evaluated the BAB-AR algorithm's applicability for different trajectories with an initial velocity of $v=100$ m/s. As shown in Fig. 20(a), acceleration of speed does not affect the accuracy of the BAB-AR algorithm, but the curvature of the trajectory can reduce the accuracy of position prediction. In Fig. 20(b), when the target MU_l turns 160° in 5s, the trajectory

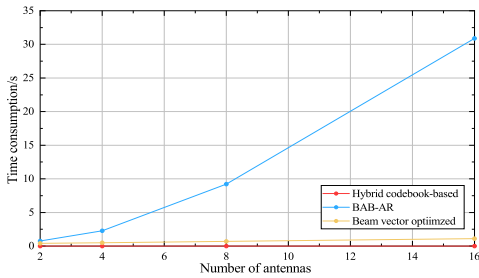


Fig. 19. Time consumption under different numbers of antennas.

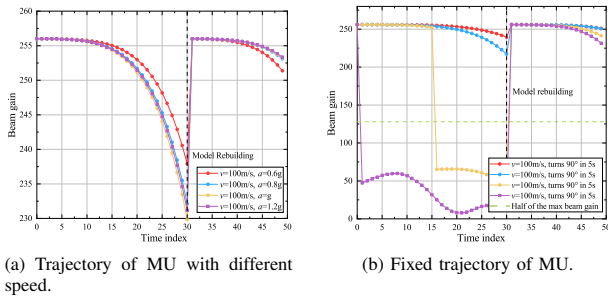


Fig. 20. Beam gain received at the MU_l with different algorithms.

from $t_n=16$ to $t_n=20$ is unrelated to the historical trajectory, and the beam gain of BAB-AR improves at $t_n=30$. However, When the MU_l turns 180° in 5s, the time required for BAB-AR to reconstruct beam cannot adapt to changes in trajectory. Because the trajectory from $t_n=0$ to $t_n=30$ has little correlation with previous trajectories. Therefore, the beam gain at the MU_l cannot exceed half of the maximum beam gain. In summary, the BAB-AR algorithm cannot adapt to MUs with too little trajectory information to predict their trajectories accurately.

VI. CONCLUSION

This study proposes an accurate beam-tracking algorithm for MUs. UAV-BSs consisting of A-UAVs and U-UAVs are employed to provide beam tracking for the MUs with adaptive beam reconstruction. U-UAVs without GPS can be located with high accuracy by A-UAVs using the proposed GDCSA algorithm. Furthermore, a TIAM is proposed for the adaptive reconstruction of the beam, and MUs can be covered with HPBW. Simulation results show that the predictive angle relative error of the GDCSA algorithm is within 0.2 under different motion patterns, which realizes a higher SNR and transmit rate at U-UAV compared to that of the angle-aware UAV beam tracking with machine model. Meanwhile, when the target MU moves fast, BAB-AR can maintains the value of beam gain at the target MU as half of the maximum beam gain that the antenna can provide. When the target MU moves slowly, the energy-efficiency at MU can be improved by up to 136.46% and 215.99% compared to that of the fixed time interval mode and the codebook-based algorithm, respectively. However, BAB-AR maynot perform effectively when the MU trajectory has a varying radian, such as the S-bend trajectory. Therefore, furture work will focus on modeling MU trajectories to improve the accuracy of beam alignment.

REFERENCES

- [1] J. Yu, Z. Yu, K. Wu, T. Lee, and Y. T. Su, "A ml-mmse receiver for millimeter wave user-equipment detection: Beamforming, beamtracking, and data-symbols detection," *IEEE Transactions on Wireless Communications*, vol. 20, pp. 5301–5313, 2021.
- [2] J. Zhao, F. Gao, W. Jia, S. Zhang, S. Jin, and H. Lin, "Angle domain hybrid precoding and channel tracking for millimeter wave massive mimo systems," *IEEE Transactions on Wireless Communications*, vol. 16, pp. 6868–6880, 2017.
- [3] Y. J. Kim and Y. S. Cho, "Beam-tracking technique for millimeter-wave cellular systems using subarray structures," *IEEE Transactions on Vehicular Technology*, vol. 67, pp. 7806–7810, 2018.
- [4] S. Jayaprakasam, X. Ma, J. W. Choi, and S. Kim, "Robust beam-tracking for mmwave mobile communications," *IEEE Communications Letters*, vol. 21, pp. 2654–2657, 2017.
- [5] J. Mu, Y. Gong, F. Zhang, Y. Cui, F. Zheng, and X. Jing, "Integrated sensing and communication-enabled predictive beamforming with deep learning in vehicular networks," *IEEE Communications Letters*, vol. 25, pp. 3301–3304, 2021.
- [6] J. Tan and L. Dai, "Wideband beam tracking in thz massive mimo systems," *IEEE Journal on Selected Areas in Communications*, vol. 39, pp. 1693–1710, 2020.
- [7] T. Feng, L. Xie, J. Yao, and J. Xu, "Uav-enabled data collection for wireless sensor networks with distributed beamforming," *IEEE Transactions on Wireless Communications*, vol. 21, pp. 1347–1361, 2022.
- [8] J. Li, G. Sun, H. Kang, A. Wang, S. Liang, Y. Liu, and Y. Zhang, "Multi-objective optimization approaches for physical layer secure communications based on collaborative beamforming in uav networks," *IEEE/ACM Transactions on Networking*, vol. 21, 2023.
- [9] Z. Wang and L. Duan, "Chase or wait: Dynamic uav deployment to learn and catch time-varying user activities," *IEEE Transactions on Mobile Computing*, vol. 22, pp. 1369–1383, 2023.
- [10] T. Taleb, A. Ksentini, H. Hellaloui, and O. Bakkouche, "On supporting uav based services in 5g and beyond mobile systems," *IEEE Network*, vol. 35, pp. 220–227, 2021.
- [11] B. Li, Z. Fei, and Y. Zhang, "Uav communications for 5g and beyond: Recent advances and future trends," *IEEE Internet of Things Journal*, vol. 6, pp. 2241–2263, 2019.
- [12] L. Zhu, J. Zhang, Z. Xiao, X. Cao, D. O. Wu, and X.-G. Xia, "3-d beamforming for flexible coverage in millimeter-wave uav communications," *IEEE Wireless Communications Letters*, vol. 8, pp. 837–840, 2019.
- [13] L. Yang and W. Zhang, "Beam tracking and optimization for uav communications," *IEEE Transactions on Wireless Communications*, vol. 18, pp. 5367–5379, 2019.
- [14] H. Song and Y. Ko, "Beam alignment for high-speed uav via angle prediction and adaptive beam coverage," *IEEE Transactions on Vehicular Technology*, vol. 70, pp. 10 185–10 192, 2021.
- [15] W. Zhang, W. Zhang, and J. Wu, "Uav beam alignment for highly mobile millimeter wave communications," *IEEE Transactions on Vehicular Technology*, vol. 69, pp. 8577–8585, 2020.
- [16] J. Zhang, W. Xu, H. Gao, M. Pan, Z. Han, and P. Zhang, "Codebook-based beam tracking for conformal array-enabled uav mmwave networks," *IEEE Internet of Things Journal*, vol. 8, pp. 244–261, 2020.
- [17] S. Hyun, J. Song, K. Kim, J. Lee, and S. Kim, "Adaptive beam design for v2i communications using vehicle tracking with extended kalman filter," *IEEE Transactions on Vehicular Technology*, vol. 71, pp. 489–502, 2022.
- [18] L. Zhu, J. Zhang, Z. Xiao, X. Cao, X. Xia, and R. Schober, "Millimeter-wave full-duplex uav relay: Joint positioning, beamforming, and power control," *IEEE Journal on Selected Areas in Communications*, vol. 38, pp. 2057–2073, 2020.
- [19] X. Chen, Z. Feng, Z. Wei, F. Gao, and X. Yuan, "Performance of joint sensing-communication cooperative sensing uav network," *IEEE Transactions on Vehicular Technology*, vol. 69, pp. 15 545–15 556, 2020.
- [20] Z. Xiao, H. Dong, L. Bai, D. O. Wu, and X. Xia, "Unmanned aerial vehicle base station (uav-bs) deployment with millimeter-wave beamforming," *IEEE Internet of Things Journal*, vol. 7, pp. 1336–1349, 2020.
- [21] C. Liu, W. Yuan, Z. Wei, X. Liu, and D. W. K. Ng, "Location-aware predictive beamforming for uav communications: A deep learning approach," *IEEE Wireless Communications Letters*, vol. 10, pp. 668–672, 2021.
- [22] Y. Huang, Q. Wu, T. Wang, G. Zhou, and R. Zhang, "3d beam tracking for cellular-connected uav," *IEEE Wireless Communications Letters*, vol. 9, pp. 736–740, 2020.

- [23] H. Song and Y. Ko, "Robust and low complexity beam tracking with monopulse signal for uav communications," *IEEE Transactions on Vehicular Technology*, vol. 70, pp. 3505–3513, 2021.
- [24] J. Zhang, W. Xu, H. Gao, M. Pan, Z. Feng, and Z. Han, "Position-attitude prediction based beam tracking for uav mmwave communications," *ICC 2019 - 2019 IEEE International Conference on Communications (ICC)*, pp. 1–7, 2019.
- [25] M. Yang, B. Ai, R. He, C. Huang, Z. Ma, Z. Zhong, J. Wang, L. Pei, Y. Li, and J. Li, "Machine-learning-based fast angle-of-arrival recognition for vehicular communications," *IEEE Transactions on Vehicular Technology*, vol. 70, pp. 1592–1605, 2021.
- [26] W. Yuan, F. Liu, C. Masouros, J. Yuan, D. W. K. Ng, and N. González-Prelcic, "Bayesian predictive beamforming for vehicular networks: A low-overhead joint radar-communication approach," *IEEE Transactions on Wireless Communications*, vol. 20, pp. 1442–1456, 2021.
- [27] M. Jiang, W. Liu, and Y. Li, "Adaptive beamforming for vector-sensor arrays based on a reweighted zero-attracting quaternion-valued lms algorithm," *IEEE Transactions on Circuits and Systems II: Express Briefs*, vol. 63, pp. 274–278, 2016.
- [28] A. Askarzadeh, "A novel metaheuristic method for solving constrained engineering optimization problems: Crow search algorithm," *Computers & Structures*, vol. 169, pp. 1–12, 2016.
- [29] H. Yan, Y. Cao, and J. Yang, "Statistical tolerance analysis based on good point set and homogeneous transform matrix," *Procedia CIRP*, vol. 43, pp. 178–183, 2016.
- [30] A. Alkhateeb, O. El Ayach, G. Leus, and R. W. Heath, "Channel estimation and hybrid precoding for millimeter wave cellular systems," *IEEE Journal of Selected Topics in Signal Processing*, vol. 8, pp. 831–846, 2014.



and optimizations.

Geng Sun (Member IEEE) received the B.S. degree in communication engineering from Dalian Polytechnic University in 2011 and the Ph.D. degree in computer science and technology from Jilin University in 2018. He was a Visiting Researcher with the School of Electrical and Computer Engineering, Georgia Institute of Technology, USA. He is currently an Associate Professor with the College of Computer Science and Technology, Jilin University. His research interests include wireless networks, UAV communications, collaborative beamforming,



Jing Zhang (Member IEEE) received the Ph.D degree in computer science and technology from Jilin University, Changchun, China, in 2015. She is Postdoctoral fellow at the College of Communication Engineering, Jilin University. Currently, she is an Associate Professor with the College of Computer Science and Technology, Changchun University of Science and Technology. Her research interests include internet of Things, blockchain, and complex network.



Sheng Gao received the B.Eng. degree in computer science and technology from Changchun University of Science and Technology, in 2021. And she is working towards the M.E. degree in Changchun University of Science and Technology from September 2021. Her research focuses on beam tracking.



Xin Feng received the Ph.D degree in computer science and technology from Changchun University of Science and Technology in 2014. He is currently a research fellow with the College of Computer Science and Technology, Changchun University of Science and Technology. His research interests include clustered storage and parallel processing, expert systems and intelligent diagnostics.



Hongwei Yang received the Ph.D degree in computer science and technology from Changchun University of Science and Technology in 2021. He is currently a Professor with the College of Computer Science and Technology, Changchun University of Science and Technology. His research interests include internet of Things, software engineering and information systems, and data Mining.